Journal of Physics: Conference Series, 2011, in press.

Presented at ETC13, Warsaw, Poland, September, 2011.

The hairpin vortex illusion

Peter S Bernard

Department of Mechanical Engineering, University of Maryland, College Park, MD 20742, USA

E-mail: bernard@umd.edu

Abstract. It has long been customary to assume that vortical structures in turbulent flows are synonymous with regions of rotational motion. Mathematical implementations of this idea using numerical and experimental velocity data from turbulent boundary layers reveal the presence of hairpin vortices, both singly and in groups called packets. However, vorticity may be present that does not directly cause rotation, and by failing to take this into account it is possible to be misled as to the true nature of the vortical structures. In this work a vortex filament scheme is applied to boundary layer flow that allows for a view of structures unrestrained by the requirement that they be regions of rotational motion. It is found that furrow-like streamwise aligned eruptions of the nominally spanwise near-wall vorticity overlying low-speed streaks are the primary structural feature of the transitioning boundary layer. These progress from an arch-like form at their upstream end to either one or two-lobed mushroom-shapes at their downstream end. The rotational motion associated with the furrows has the appearance of hairpins. Mushroom-shaped structures rapidly breakdown into complex forms in the post-transitional region that may have rotational signatures similar to that of packets.

1. Introduction

The "hairpin vortex" that figures prominently in discussions of transitioning and turbulent boundary layers (Adrian, 2007), is conceptualized as being a condensed region of rotational motion in a shape reminiscent of a "hairpin." Such vortical objects tend to have "legs" in the shape of parallel counter-rotating vortices connected via an "arch" or "horseshoe" shaped vortex. The concept has a long history (Theodorsen, 1952), fits into a great many theoretical descriptions of how the boundary layer might work and has been used to explain a diverse set of quantitative measurements and qualitative visualizations. Direct evidence for the existence of hairpins both alone and in groups called "packets" has been found by using appropriate scalar markers (Chakraborty *et al.*, 2005) to plot isosurfaces of rotational motion obtained from three-dimensional grids of velocity data produced by direct numerical simulations (Adrian & Liu, 2002; Wu & Moin, 2009), large eddy simulations (Schlatter *et al.*, 2006) and tomographic particle image velocimetry in laboratory flows (Gao *et al.*, 2010; Schroder *et al.*, 2008; Elsinga *et al.*, 2010; Sheng *et al.*, 2009; Katz & Sheng, 2010).

While the definition of a "vortex" as a region of rotational motion leads to the discovery of many dynamically important hairpin-shaped "vortices" in the boundary layer, it is another matter to conclude that such hairpins are actually composed of vorticity in a comparable shape that can be taken to be a bona fide hairpin structure. In particular, though vorticity is generally

necessary for the presence of rotational motion, it cannot be said that rotational motion itself must be uniquely connected to a vortical structure of one sort or another. In fact, vorticity that is not directly involved in creating rotational motion cannot be ruled out from having an important role to play in structures that do have rotational motion. Focusing on just rotational motion within a flow is liable to give a distorted and perhaps even entirely false impression as to the make up of the true structures.

One effective means for exposing the complete local accumulation of vorticity that underlies hairpin-shaped regions of rotational motion is via computations using vortex filaments (Bernard, 2006). Unlike gridded vorticity data that may be available from experiment or computation, the vortex filaments have circulation and freely arrange themselves to form clearly identifiable structure. In essence, filaments supply information about the strength and orientation of vorticity that lies at the heart of what a structure is conceptualized to be. This idea has been used often in the analysis of free shear flows such as mixing layers (Ashurst & Meiburg, 1988; Bernard, 2008) and jets (Martin & Meiburg, 1991; Bernard, 2009) and can be applied in boundary layer simulations once proper attention is paid to the production of vorticity within the near-wall sublayer. A scheme with these properties has been developed and recently applied to the simulation of a spatially growing boundary layer (Bernard *et al.*, 2010). A conclusion of this study − that is further explored in the present work − is that, in fact, the nature of the boundary layer structure cannot be understood without taking into account the essential role of vorticity that is not directly involved in rotation. Failure to consider the role of this vorticity in boundary layer physics has led to the illusion that hairpin vortices and packets are structures in their own right.

2. Vortex Filament Scheme

The present discussion is primarily illustrated using vortical structure obtained specifically from within the transition region of a spatially developing boundary layer where coherent events are considerably easier to describe than in the fully turbulent zone. In fact, the prototypical structural features of near-wall boundary layers consisting of low speed streaks with accompanying vortical motions are, in their basic outlines, common to both transitional and turbulent flows. Consequently, insights gained in transition should have considerable weight in understanding the dynamics of the fully turbulent region itself. This viewpoint has guided much previous analysis of hairpin-shaped structures, where it is believed that the mechanisms leading to hairpin and hairpin packet formation are common to both transition and turbulence. It is also the case that the dynamics of vortical structures within transition is of interest in its own right since such phenomena have a natural tie-in to the propagation of secondary instabilities on low speed streaks during bypass transition (Brandt *et al.*, 2004).

The spatially developing boundary layer simulations that provide the basis for this work include a substantial transition region preceding the onset of turbulence. The flow is past a wide and somewhat streamlined flat plate of scaled dimensions in the streamwise, normal and spanwise (x, y, z) directions of 1.5, .05 and 2.5, respectively. The Reynolds number at the downstream edge of the plate varies in different calculations from 75,000 to 120,000. Just the flow within the central region $|z| \leq 0.25$ of the plate, where the mean field is two-dimensional and is unaffected by flow at the lateral edges, is used for analysis. In a typical simulation this reduced domain is more than five boundary layer thicknesses wide and has approximate dimensions in wall units of 4890 and 1630 in the streamwise and spanwise directions, respectively.

The surface of the plate is represented via a grid of up to 98,088 triangles. A thin prismatic mesh of thickness 0.012 subdivided into 11 levels is erected over the surface within which the vorticity transport equation including all viscous effects is solved via a finite volume scheme. Vorticity appearing at the top of the mesh is converted into new vortex tubes with a circulation

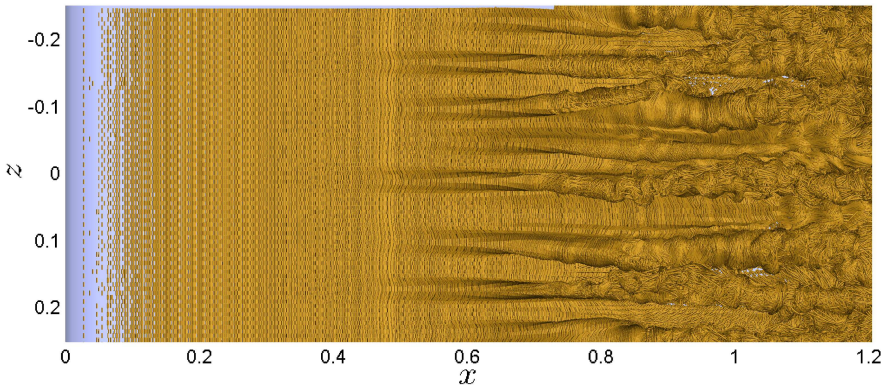

Figure 1. Overhead view of vortex filaments in the boundary layer simulation showing the formation of vortex furrows as the flow transitions to turbulence.

determined so as to maintain the identical long range velocity. The vortex tubes convect via their end points with an unchanging circulation. As they stretch they are subdivided. Vortex loops forming out of the filaments within the turbulent part of the boundary layer are removed thus providing a de facto subgrid model that provides intermittent dissipation without interference to the backscatter process (Bernard, 2006). Filaments that convect beyond the position $x = 1.75$ are removed from the computation. Many details about the methodology, particularly in the present case containing bounding surfaces, may be found in Bernard *et al.* (2010). For the boundary layer flow, predictions of mean velocity range from a Blasius boundary layer profile upstream of transition to a log law matching experiments and computations in the fully turbulent zone. In addition to the boundary layer, validation of the statistical predictions of the filament scheme have been demonstrated in canonical flows such as a shear layer (Bernard, 2008) and jet (Bernard, 2009).

3. Boundary Layer Structure

Some idea of what the boundary layer simulation entails is given in Fig. 1 showing the computed vortex filament field at a fixed time viewed from above. At the left is the rounded leading edge of the plate at $x = 0$. Here the flow is fully laminar with vorticity only contained in the surface mesh (not visible). A short distance downstream as the boundary layer thickens vortex filaments appear that are oriented exclusively in the spanwise direction. Midway in the image the flow begins to undergo transition that is fully achieved somewhat before the right boundary of the picture at $x = 1.2$. Downstream of this location the flow is fully turbulent everywhere.

The image in Fig. 1 shows that the filaments have a significant capacity to organize into visible structure, both in the transition and turbulent regions. In the former they are formed into streamwise-oriented furrow-like raised vortex filaments that grow in prominence before devolving into a more disorganized state in the turbulent region. Even where the flow is turbulent the filaments tend to be somewhat organized into distinct groupings that interact with each other in complex ways. Before considering in detail the nature of the structures revealed by the filaments it is helpful to place the view in Fig. 1 into a more traditional context. This is given in Fig. 2 which, for the identical domain as in Fig. 1, shows isosurfaces of quantities commonly used in describing the boundary layer structure. In particular, indicated in blue are isosurfaces of slow moving fluid with streamwise velocity fluctuation $u = -0.3$, faster moving fluid with $u = 0.125$ indicated in red and isosurfaces of rotational motion in green. The latter are determined via the

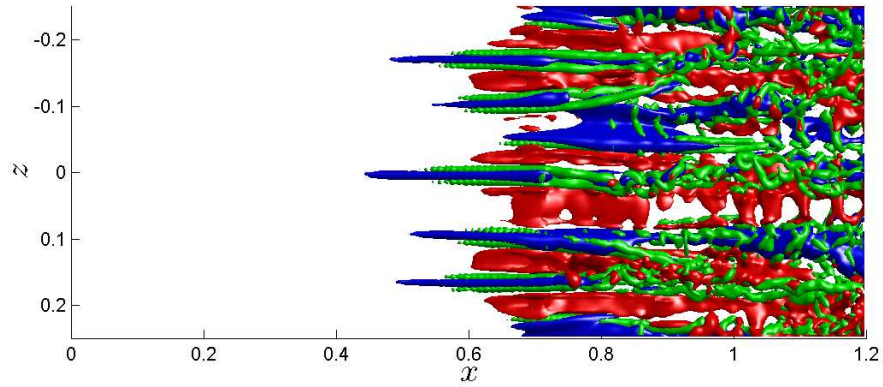

Figure 2. Isosurfaces of rotation (green) and positive (red) and negative (blue) isosurfaces of streamwise velocity fluctuation for the same view as in Fig. 1.

second eigenvalue, λ_2, of the matrix formed from the sum of the squares of the rate of strain and rotation tensors – a quantity that is associated with the presence of local rotation (Chakraborty *et al.*, 2005). In the present case λ_2 is found by first evaluating the velocity field on a mesh and then computing the necessary derivatives via finite difference formulas. The value $\lambda_2 = -100$ is used in this figure. Values of λ_2 within a significant range of this give virtually identical results.

Within the region $0.5 \leq x \leq 0.9$, Fig. 2 shows the presence of streaks of low speed fluid being ejected outward from within the apparent legs of hairpin-shaped regions of rotational motion. Parallel to and outside the hairpins lie streak-like incursions of high speed fluid. A closer view of the relationship between the velocity streaks and the hairpins is given in Fig. 3. The low speed fluid is seen to be confined and uplifted within a relatively narrow band ejecting between the hairpin legs, while a broader region of high speed fluid fills in the region close to the wall on either side of the hairpins. The spacing between streaks in wall units in Fig. 2 varies between approximately $\Delta z^+ \approx 150$ and 225 and the streamwise extent of the transition zone is approximately $\Delta x^+ = 1100$. These properties are not unlike the Klebanoff mode of transition as has been previously observed. It should be noted that in the present case, since no overt forcing is applied, the appearance of the Klebanoff transition mode must be attributed to an innate sensitivity of the vortex discretization to slight spanwise perturbations. In fact, small spanwise variations in velocity can already be detected in the flow within the prism mesh upstream of the first appearance of filaments. Evidently, such perturbations trigger the downstream transformation of the vortex system via a de facto bypass transition. The rapidity with which the vortices break down into turbulence depends to some extent on the Reynolds number and the nature of the upstream flow. For example, by replacing the viscous calculation in the rounded front of the plate by inviscid flow, transition can be significantly delayed.

A direct comparison of Fig. 1 with Fig. 2 suggests that the structural features in the two figures have a one-to-one correspondence. Thus, the furrows formed from filaments in Fig. 1 lie at the same locations as the low-speed streaks plus their associated hairpin-like regions of rotational motion in Fig. 2. The high speed incursions are in the regions adjacent to and outside the furrows. It is clear that the arrangement of vortex filaments within the furrows must be responsible for the low speed streaks and the apparent hairpin-like regions of rotational motion that accompany them. By examining the furrows in detail, it becomes possible to gain new insights into the vortical structure of the boundary layer.

Figure 4 contains a closeup view looking upstream of the filaments composing two furrows.

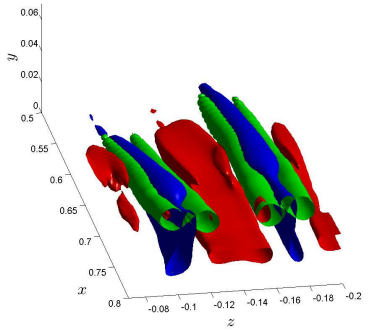

Figure 3. Detail of Fig. 2.

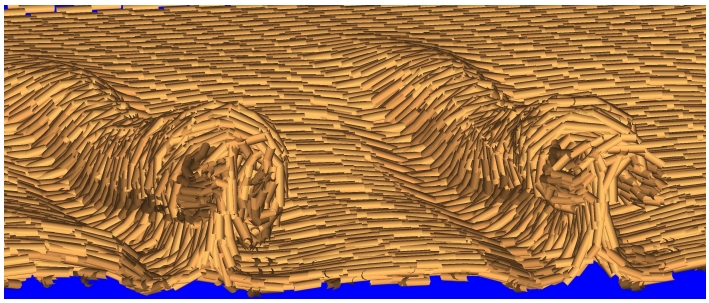

Figure 4. Upstream view of vortex filaments showing the spatial makeup of furrows.

The furrows have been severed at the downstream end in the foreground revealing some notion of their inner details. It is seen that the vortex furrows develop gradually from initially forward-tilted arch-like filaments at the upstream end to become mushroom-like arrangements at the downstream end. An example of how this structure matches up with the regions of rotational motion is given in Figs. 5 and 6 where filaments intersecting several narrow planes along a furrow are plotted with isosurfaces of λ_2. Figure 5 is a view of the upstream end of a furrow with contours rendered transparent to show how they exactly intersect the forward tilted arch-like vortices. Vortex filaments at locations between those that are shown have the identical profiles. It is clear that counter-rotating motion that produces the hairpin legs originates in the streamwise projection of the continuous sequence of upraised and forward tilted vortices that are arrayed along the length of the furrows in this location.

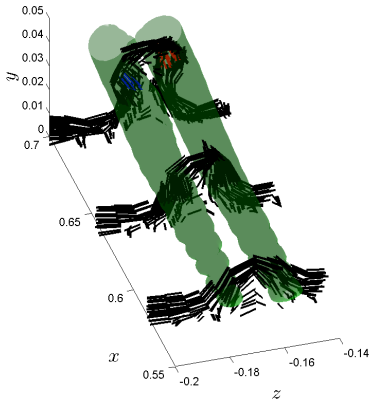

Figure 5. Filaments and isosurfaces of rotation near the onset of furrows.

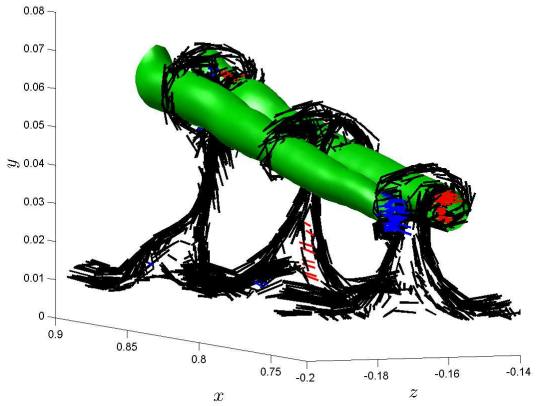

Figure 6. Isosurfaces of rotation intersect the lobes of mushroom-shaped filaments.

Especially interesting, as shown in Fig. 6, is the upstream extension of the furrow in Fig. 5 into the region where the filaments have taken on the mushroom-shaped appearance. Figure 6 brings into sharp relief the fact that the iso-surfaces of rotational motion go through the lobes of the mushrooms that are now the centers of the counter-rotating motion. Vortex tubes that are within pi/16 radians of the streamwise direction are indicated as red or blue depending on whether they are oriented in the positive or negative streamwise directions, respectively. Such vorticity is at the center of the lobes and within the hairpin legs suggesting that the latter have vorticity aligned along their axes. Consistent with the fact that hairpins are often observed to occur with a single "leg," (referred to as "canes") similar structures are not uncommon in

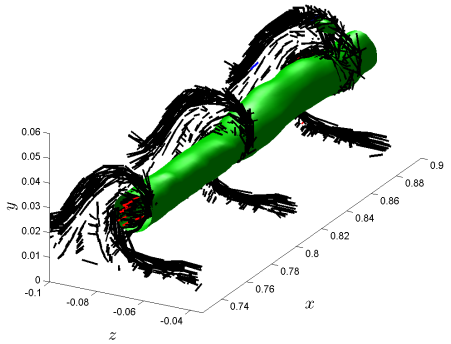

Figure 7. A single-lobed mushroom develops downstream from tilted arch-like filaments.

the filament simulation. An example is shown in Fig. 7 where it is seen that the single leg of a hairpin intersects vortex filaments in the shape of a single-lobed mushroom. This behavior occurs in furrows for which the arches at the upstream end have tilted strongly to one side or the other. The lobe closest to the ground subsequently develops into the form seen in the figure while the external lobe atrophies.

Whether the hairpin legs appear singly or in counter-rotating pairs, Figs. 6 and 7 make clear that there is much non-rotational vorticity engaged in the functioning of the vortical structures that produce hairpins. This includes vorticity normal to the boundary forming the stem-like structure below the mushrooms as well as spanwise vorticity that spreads across the top. Apparently, such vorticity is reoriented and stretched by the counter-rotating motion causing it to work its way into eventually accumulating within the lobes of the mushrooms. For this reason, despite the fact that hairpin legs may at times contain a preponderance of streamwise vorticity directed along their axes, they nonetheless cannot be regarded as structures in their own right. The actual structures, whose dynamics are an essential part of the boundary layer physics, consist of the furrows made up of the hairpin legs together with the vorticity acting in a supporting role.

4. Dynamics

The vortex furrows are relatively long-lived and occupy an approximately stable position within the boundary layer consistent with the observed longevity and persistence of low speed streaks. For example, within the current simulation, during an elapsed time of $\Delta t^+ = 320$, a complete changeover of essentially one furrow takes place. At the same time, the filaments of which the furrows are composed continuously convect downstream so that it must be the case that filaments pass along and within the length of the furrows and as they do so they develop from arch into mushroom-shaped structures as if in an assembly line. This point is supported by Fig. 8 showing the development of a mushroom from an upstream arch as seen from the perspective of an observer moving with the convection velocity 0.7 of the free stream. The appropriateness of this speed can be deduced from considering the motion of maxima of the space/time correlations of the velocity field within the furrows, and fits in with similar convection velocities deployed in the analysis of hairpin structure (Adrian, 2007). Thus, the small arch in Fig. 8(a) at a reference time of 0, progresses through the states indicated in (b) and (c) over the elapsed time $\Delta t^+ = 42.5$ by which time it acquires the appearance of a mushroom. It should also be remarked that there is a distinct similarity between the spatial progression of the filament images in Figs. 5 and 6 at a fixed time, and the time evolution in Fig. 8. This connection is particularly evident in the development of the wall-normal vorticity within the mushroom stems where the raised sides of

the arches are pushed in toward each other as the top of the mushroom ejects outward together with low-speed fluid.

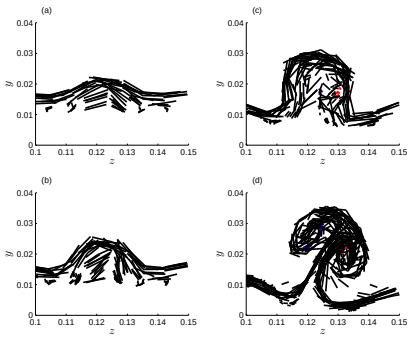

Figure 8. Filaments in a furrow viewed by a moving observer. Relative times are at $t^+ = 0$, 10.6, 23.4 and 42.5.

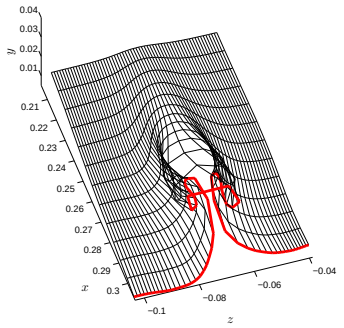

Figure 9. Bubble wire signature of a furrow.

Another viewpoint with which to examine the dynamics is from a visualization of simulated microbubbles or smoke. Bubble wire images are readily imitated numerically by calculating the paths of tracer particles released along spanwise lines in the simulation. Figure 9 shows one such result for tracers released on the plane $y^+ = 50$ spanning a single furrow. The lines in the flow direction within the image represent streaklines that connect particles coming out of the same point at different times, while the spanwise lines connect the cohort of particles that are placed into the flow at each time step. Together they represent the sheet of bubbles or smoke that has entered into the numerical flow. It is seen that the furrow strongly affects the movement of the particles via the associated counter-rotating motion. Thus, particles are slowed down as they are ejected up through the center of the furrow and speeded up as they are swept laterally to the side and rolled up into the lobes. This motion is particularly evident in the highlighted, red line that represents the set of particles that were first released into the flow.

The pattern in Fig. 9 appears to be that of a "pocket," such as is commonly observed in smoke-marked boundary layers (Falco, 1991). If this is the case, then it is evident that the pockets must reflect the action of the furrows upon the scalar markers. The particles rise up and spread laterally across the top of the furrow creating the "scoured" appearance in the figure as well as concentrate particles into the lobes creating the impression of a distinctive edging to the pocket. The tapered downstream end of the pockets reflects the fact that the longer the particles are under the influence of the furrow, the more they are circulated around the lobes.

The shape of the tracers in Fig. 9 has a strong connection to the observed time evolution of the vortex filaments in Fig. 8. Thus, initially spanwise vorticity in the near-wall layer is reoriented into the normal direction where it is drawn up through the center of the counter-rotating motion and slowed relative to the adjacent fluid. Lateral stretching of the vorticity across the top of the mushroom together with its acceleration by the faster moving fluid across the top shear layer leads to reorientation into the streamwise direction that reinforces the motion that creates the counter-rotating velocity field that drives the process. Thus, the furrow-like structure is self-reinforcing in the sense that it efficiently uses counter-rotating motion produced by streamwise vorticity to further enable the process by which streamwise vorticity is generated.

The continuous progression of vorticity in the furrows from arches to mushrooms acts in concert to produce the counter-rotating motion that leads to the creation of low-speed streaks. Since hairpin-shaped regions of rotational motion generally appear with the furrows, an explanation is thus provided for the association between isolated hairpins and low-speed streaks.

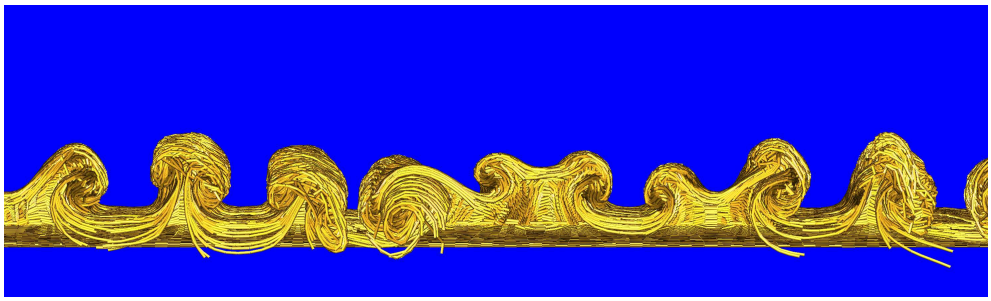

Figure 10. End-on view of vortex filaments near the end of transition.

In particular, there is no need to conjecture the necessity of having multiple hairpins acting in unison within the context of packets in order to produce them (Adrian, 2007).

5. The End of Transition

A view of the filaments on a cut across the boundary layer at a point within the late transition is given in Fig. 10 for a typical simulation. This shows that a variety of disturbances are beginning to act to disrupt the inherent organization of the furrows. Thus, it is may be seen that some of the mushrooms have tilted sideways at large angles, others are now essentially single-lobed structures and others have become somewhat disordered in appearance. With tilting the two lobes of the mushrooms experience quite different flow conditions. For the one closest to the surface, vorticity in the near-wall layer appears to have a tendency to wrap around the lobe. In contrast, the outer lobe experiences augmented shearing against the high speed fluid of the outer flow that potentially promotes roll-up of the stretched vorticity into vortices with the appearance of arches.

Some insight into how the furrows finally breakdown into turbulence may be gleaned from Fig. 11 that shows, at a fixed time, profiles of the filaments at several streamwise positions. The organization into mushrooms that is largely intact in the lowest image is virtually non-existent in the top figure. During the spatial extent between these locations in the flow several of the mushrooms tilt over to the point of propagating directly into the wall vorticity. Others, such as those at $z = -0.175$ and 0.01 have twisted sideways. The structures at z=0.1 and 0.16 have entered into a strong interaction that seemingly is initiated by the tilting of the mushrooms toward each other.

As mentioned above, vorticity passes through the furrows in more or less highly correlated groupings so that when the downstream end is reached discrete vortices with forms like those seen in Figs. 10 and 11 are released into the post-transitional field. The complexity of such vortices rapidly increases to the point where they are difficult to describe in detail, though they share many common vortical features. It is especially difficult to forge a clear link between the filament structure and the associated isosurfaces of rotational motion. Some indication of this is evident in Figs. 1 and 2. As a specific example, consider Fig. 12 taken from the simulation at $R_e = 120,000$ that shows what appears to be several nested hairpins overlying a low-speed streak. However, the form taken by the filaments within each of the arch-like rotational regions, shown in Fig. 13, is not unlike those seen previously in the furrows. In fact, the structure responsible for Fig. 12 is a tilted furrow wherein the streamwise vorticity along the outer surface has experienced sufficient shearing to cause its roll-up and thus the impression that arch-like vortices are present.

The post transitional structures maintain a degree of streamwise coherence even as they

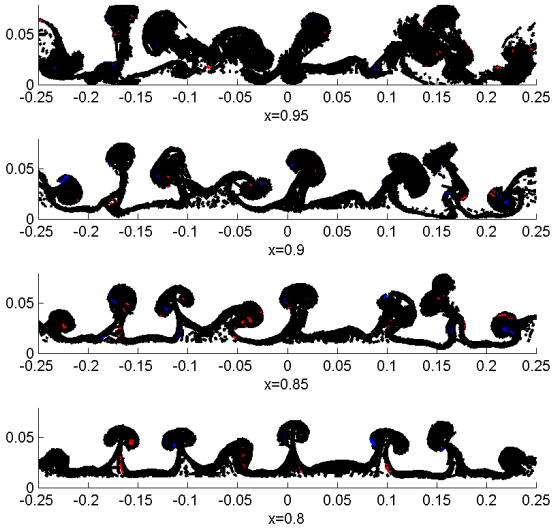

Figure 11. Filaments at a fixed time showing progression to turbulent flow at the end of transition.

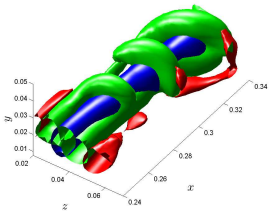

Figure 12. Isosurfaces of λ_2 reminiscent of a hairpin packet.

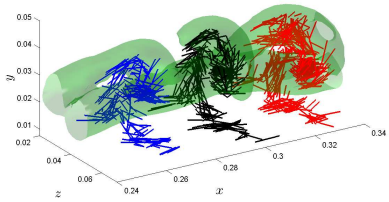

Figure 13. Filaments underlying the arch-like structure in Fig. 12.

convect downstream and gain in complexity. This kind of correlation may contribute to the appearance of identifiable patterns within the turbulent field, such as that ascribed to the existence of hairpin packets. However, the supposition that actual hairpins vortices do exist within packets is called into question by the fundamental uncertainty, such as illustrated in Figs. 12 and 13, as to what particlar arrangements of filaments underlie rotational regions in the flow.

6. Conclusions

Simulation of the spatially growing boundary layer has been performed using a hybrid vortex filament scheme that reveals the form of coherent vortices without the need to define structure as being regions of rotational motion. Objects with the shape of hairpin vortices are found not to be actual structures in their own right, but rather the rotational signatures of elongated furrow-like eruptions in the surface vortex layer. While the furrows are long-lived, vorticity within them convects quickly downstream progressing from an arch-like to a one or two-lobed mushroom-like state. Mushroom-shaped structures leaving the furrows into the post-transitional region tilt, twist, interact with the wall vorticity and neighboring structures and thus develop into complex, semi-coherent forms as they move downstream into the fully turbulent region. As in the case of individual hairpins, iso-surfaces of rotational motion are found not to be a reliable

indicator of the form taken by the underlying vortex structure. Consequently, the existence of structural forms in the turbulent boundary layer such as the system of hairpins in the packet model, that are based primarily on identifying regions of rotational motion, may be illusory.

Acknowledgments

This research was supported in part by the National Science Foundation through TeraGrid resources provided by the Pittsburgh Supercomputing Center.

References

Adrian, R. J. 2007 Hairpin vortex organization in wall turbulence. *Phys. Fluids* **19**, 041301.

Adrian, R. J. & Liu, Z.-C. 2002 Observation of vortex packets in direct numerical simulation of fully turbulent channel flow. *J. Visualization* **5**, 9–19.

Ashurst, W. T. & Meiburg, E. 1988 Three-dimensional shear layers via vortex dynamics. *J. Fluid Mech.* **189**, 87–116.

Bernard, P. S. 2006 Turbulent flow properties of large scale vortex systems. *Proc. Nat'l. Acad. Sci.* **103**, 10174–10179.

Bernard, P. S. 2008 Gridfree simulation of the spatially growing mixing layer. *AIAA J.* **46**, 1725–1737.

Bernard, P. S. 2009 Vortex filament simulation of the turbulent coflowing jet. *Phys. Fluids* **21** (025107).

Bernard, P. S., Collins, P. & Potts, M. 2010 Vortex filament simulation of the turbulent boundary layer. *AIAA J.* **48**, 1757–1771.

Brandt, L., Schlatter, P. & Henningson, D. S. 2004 Transition in boundary layers subject to free-stream turbulence. *J. Fluid Mech.* **517**, 167–198.

Chakraborty, P., Balachandar, S. & Adrian, R. J. 2005 On the relationships between local vortex identification schemes. *J. Fluid Mech.* **535**, 189–214.

Elsinga, G. E., Adrian, R. J., van Oudheusden, B. W. & Scarano, F. 2010 Three-dimensional vortex organization in a high-reynolds number supersonic turbulent boundary layer. *J. Fluid Mech.* **644**, 35–60.

Falco, R. E. 1991 A coherent structure model of the turbulent boundary layer and its ability to predict reynolds number dependence. *Phil. Trans. Roy. Soc. A* **336**, 103–129.

Gao, Q., Ortiz-Duenas, C. & Longmire, E. K. 2010 Eddy structure in turbulent boundary layers based on tomographic piv. In *15th Int. Symp. on Applications of Laser Techniques to Fluid Mechanics*, pp. 1–12.

Katz, J. & Sheng, J. 2010 Applications of holography in fluid mechanics and particle dynamics. *Ann. Rev. Fluid Mech.* **42**, 531–555.

Martin, J. E. & Meiburg, E. 1991 Numerical investigation of three-dimensionally evolving jets subject to axisymmetric and azimuthal perturbations. *J. Fluid Mech.* **230**, 271–318.

Schlatter, P., Stolz, S. & Kleiser, L. 2006 Large-eddy simulation of spatial transition in plane channel flow. *J. Turbulence* **7** (33).

Schroder, A., Geisler, R., Elsinga, G. E., Scarano, F. & Dierksheide, U. 2008 Investigation of a turbulent spot and a tripped turbulent boundary layer flow using time-resolved tomographic piv. *Exp. Fluids* **44**, 305–316.

Sheng, J., Malkiel, E. & Katz, J. 2009 Buffer layer structures associated with extreme wall stress events in a smooth wall turbulent boundary layer. *J. Fluid Mech.* **633**, 17–60.

Theodorsen, T. 1952 Mechanism of turbulence. In *Proc. Midwestern Conf. Fluid Dyn.*. Ohio State University, Columbus, Ohio.

Wu, X. & Moin, P. 2009 Direct numerical simulation of turbulence in a nominally zero-pressure-gradient flat-plate boundary layer. *J. Fluid Mech.* **630**, 5–41.